Estimation of Thermoelastic Behavior of Three-phase: AA1100/Ni-Coated Boron Carbide Nanoparticle Metal Matrix Composites

A. Chennakesava Reddy

Abstract— The objective of the present work was to estimate non-linear thermoelastic behavior of three-phase AA1100/Ni-coated B_4C metal matrix composites. The thermal loading was varied from subzero temperature to under recrystallization temperature. The RVE models were used to analyze thermo=elastic behavior. the load bearing capacity of AA1100/Ni-coated B_4C composite was reduced with increase of temperature. The elastic and thermo-elastic strains were high in the direction of tensile loading for temperatures higher than 0^oC whereas these were high in the direction normal to tensile loading for temperatures lower than or equal to 0^oC. As the temperature increased ductile mode of failure was witnessed in the composites.

Index Terms— AA1100, Boron carbide, Ni-coating, three phase, RVE model.

1. Introduction

BORON carbide (B_4C) nanoparticles of 10-100 nm have specific surface area of 10-75 m^2/g. Boron carbide has several elegant properties, such as high strength, high stiffness, high hardness, high temperature and wear resistance, anti-oxidation, and good self-lubrication. This is widely used in the field of composite materials to produce blasting nozzles and bearings. This is also used to produce bulletproof armor which is suitable for lightweight bulletproof armor.

The existence of high modulus particulates can promise superior mechanical properties of metal matrix composites [1], [2]. The thermo-mechanical behavior of particulate metal matrix composites is synchronized by its microstructures such as particle properties, size and distribution. Numerous models have been developed to predict the effective material properties of particulate metal matrix composites using the homogenization theories. The Mori–Tanaka (M–T) theory has been proven to provide reasonable predictions for the effective material properties of two-phase composites. Doghri and Friebel [3] have predicted the effective elastoplastic properties of SiC whisker-reinforced aluminum matrix composites with various volume fractions. The results from the M–T theory were consistent with the experimental data. Duschlbauer et al. [4] have implemented an extended M–T scheme for modeling the linear thermoelastic behavior of carbon fiber reinforced copper matrix composites. Nevertheless, the M–T theory failed to give good estimates for the localization effect induced by the microstructures.

Finite element method (FEM) is competent of identifying the local response of the material. A general practice to determine the bulk and local responses of composite material is to employ a unit cell reinforced by a single fiber, whisker or particle subjected to periodic and symmetric boundary conditions [5].

The objective of the present work was to estimate non-linear thermoelastic behavior of three-phase (i.e. metal matrix, nanoparticle and coating on nanoparticle) composites. Nickel (Ni) coated B_4C nanoparticles were employed to fabricate AA1100/B_4C metal matrix composites. The RVE models were used to analyze the AA1100/AlN nanoparticulate metal matrix composites with interphase between B_4C nanoparticles and AA100 matrix alloy using finite element analysis. The thermal loading was varied from subzero temperature to under recrystallization temperature. The results obtained from the finite element analysis were verified with those obtained from the experimentation.

2. Mori–Tanaka Theory

The representative volume element (RVE) contains a matrix phase, denoted by a subscript m, a reinforcement phase, represented by a subscript p and an interphase between particle and matrix, represented by a subscript i. The volume fractions (V_i) of these three phases led to $V_m + V_p + V_i = 1$. The domain of RVE is denoted by ϖ.

In thermo-elasticity, the mean strain over all reinforced nanoparticles is related to the macroscopic strain ε and a uniform change in temperature ΔT as

$$\langle \varepsilon \rangle_{\omega p} = A^{\epsilon} : E + \alpha^{\varepsilon} \Delta T \quad (1)$$

where a colon designates a tensor product contracted over two indices and the brackets $\langle\ \rangle$ represent a volume average. A^{ε} and B^{ε} are two strain concentration tensors. The relationship between A^{ε} and B^{ε} is given by:

$$A^{\epsilon} = B^{\epsilon} : \left[\left(V_i + V_p \right) B^{\epsilon} + \left(1 - V_i - V_p \right) I \right]^{-1} \quad (2)$$

where I designates the fourth-order symmetric identity tensor.

A. Chennakesava Reddy is currently Proffesor and BOS Chairman, Department of Mechanical engineering, JNT University Hyderabad, India, Mobile-09440568776. E-mail: acreddy@jntuh.ac.in

For M–T model, the strain concentration tensor B^{ε} is given by

$$B^{\epsilon} = \left[I + \xi_{(I,C_m)} : \left\{(C_m)^{-1} : C_i + C_p - I\right\}\right]^{-1} \quad (3)$$

where $\xi_{(I,C_m)}$ is Eshelby's tensor and depends on the geometry of inclusion and matrix stiffness.

$$\alpha^{\varepsilon} = (A^{\varepsilon} - I) : \left(C_p + C_i - C_m\right)^{-1} : \left(\beta_p + \beta_i - \beta_m\right) \quad (4)$$

$$E = V_m \langle\varepsilon\rangle_{\omega_m} + V_i \langle\varepsilon\rangle_{\omega_i} + + V_p \langle\varepsilon\rangle_{\omega_p} \quad (5)$$

where, β = –C:a and a is the coefficient of thermal expansion (CTE).

The effective strength of the composite can be computed:

$$\langle\sigma\rangle = \bar{C} : E + \bar{\beta}\Delta T \quad (6)$$

where the effective bulk stiffness $\bar{C}$ is found as

$$\bar{C} = \left[\left(V_p C_p, V_i C_i\right) : B^{\varepsilon} + \left(1 - V_p - V_i\right) C_m\right] : \left[V_p B^{\varepsilon} + \left(1 - V_p - V_i\right)\right]^{-1} \quad (7)$$

where,

$$\bar{\beta} = V_m \beta_m + V_p \beta_p + V_i \beta_i + V_p C_p + V_i C_i - V_m C_m : \alpha^{\varepsilon} \quad (8)$$

3. Materials and Methods

The matrix material was AA1100 aluminum alloy. The reinforcement material was Ni coated B_4C nanoparticles of average size 100nm. The mechanical properties of materials used in the present work are given in table 1.

The composites were prepared by the stir casting technology and low pressure die casting process [6]. The volume fractions of Ni coated B_4C nanoparticles were 10%, 20% and 20%. The as-cast samples were heat treated under H14 conditions. The tensile properties were established as per ASTM D3039 standard test procedure. The test samples were observed under a scanning electron microscope (SEM) to establish the interphase mechanisms governing the thermo-elastic behavior of nanoparticle metal matrix composites.

TABLE 1
MECHANICAL PROPERTIES OF AA1100 MATRIX, B_4C NANOPARTICLES AND NICKEL

Property	AA1100	B_4C	Ni
Density, g/cc	2.78	2.51	8.89
Elastic modulus, GPa	69	445	207
Ultimate tensile strength, MPa	483	155	317
Poisson's ratio	0.33	0.19	0.31
CTE, µm/m-°C	21.8	5.6	13.1
Thermal Conductivity, W/m-K	220.0	90.0	60.7
Specific heat, J/kg-K	904	1288	460

In this research, a square RVE (figure 1) was implemented to analyze the tensile behavior AA1100/B_4C nanocomposites. The loading on the RVE was defined as symmetric displacement, which provided equal displacements at both ends of the RVE. The large strain PLANE183 element was used in the matrix and the interphase regions in all the models (table 1). In order to model the interphase between nanoparticle and matrix, a CONTACT172 element was used. The maximum contact friction stress of $\sigma_y/\sqrt{3}$ (where, σ_y is the yield stress of the material being deformed) was applied at the contact surface (figure 2). The basic Coulomb friction model was considered between two contacting surfaces which could carry shear stresses up to a certain magnitude across their interface before they start sliding relative to each other. This state is known as sticking. The Coulomb friction model defines an equivalent shear stress at which sliding on the surface begins as a fraction of the contact pressure P. Once the shear stress is exceeded, the two surfaces would slide relative to each other. This state is known as sliding. Both uniform thermal and hydrostatic pressure loads were applied simultaneously on the RVE model. The uniform temperature was varied from subzero to below recrystallization temperature of AA1100.

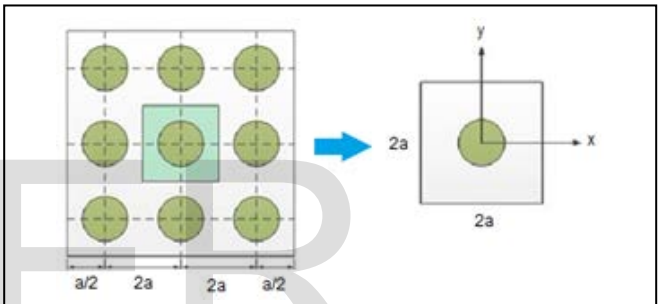

Fig. 1. A square RVE containing a nanoparticle.

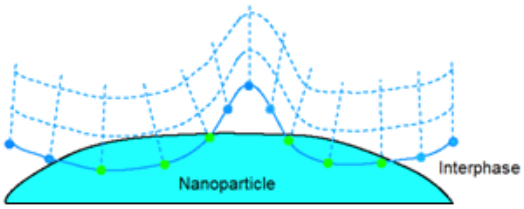

Fig. 2. Interphase contact model.

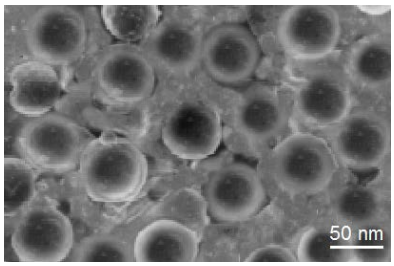

Fig. 3. Ni-coated B_4C nanoparticle distribution in AA1100 matrix.

4. Results And Discussion

A near-uniform distribution of Ni-coated B_4C nanoparticles in AA1100 matrix was observed (figure 3). This was due to marginal difference of density between matrix and

coated nanoparticles. The densities of B_4C nanoparticle and AA1100 are, respectively, 2.51 and 2.71 g/cc. Due to Ni coating the density of B_4C nanoparticle was raised to 3.02 g/cc. The Ni coating was clearly observed around the B_4C nanoparticles.

4.1 Thermo-elastic Behavior

Figure 4 illustrates the influence of hydrostatic and temperature on the elastic and thermo-elastic strains developed in the composites. The elastic strain was due to structural loads only; whereas thermo-elastic strain (= elastic strain + thermal strain) was on account of structural and thermal loads. The elastic strain decreased with increase of hydrostatic pressure (figure 4a) owing to transfer of load from matrix to stiffer B_4C nanoparticle. The thermo-elastic strain increased with increase of temperature (figure 4b). During experimentation, it was noticed that the load bearing capacity (amount of hydrostatic pressure) of AA1100/Ni-coated B_4C composite was reduced with increase of temperature.

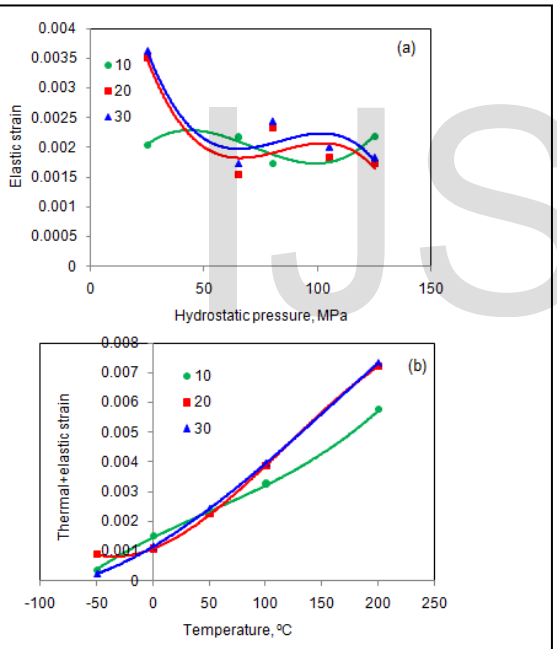

Fig. 4. Influence of hydrostatic pressure and temperature respectively on elastic and thermo-elastic strains.

Figure 5 demonstrates the state of elastic and thermo-elastic strains developed in the AA1100/Ni-coated B_4C composites having 10% volume fraction (V_p) of Ni-coated B_4C nanoparticles. In all the cases Ni-coated B_4C nanoparticles had experienced the compressive stains. This can be attributed CTE mismatch between the matrix and the Ni-coated B_4C nanoparticles. For Ni-coated B_4C nanoparticles the CTE is lower than that of AA1100 matrix. The elastic and thermo-elastic strains were high in the direction of tensile loading for temperatures higher than 0°C whereas these were high in the direction normal to tensile loading for temperatures lower than or equal to 0°C.

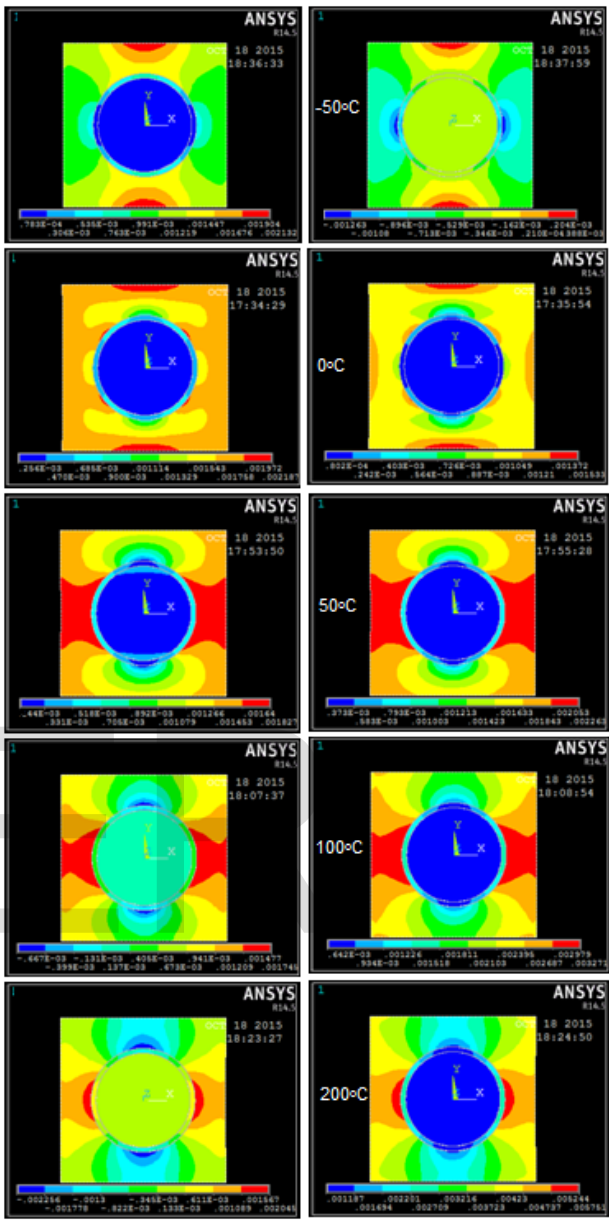

Fig. 5.Elastic and thermo-elastic strains developed in composites with10%Vp nanoparticles.

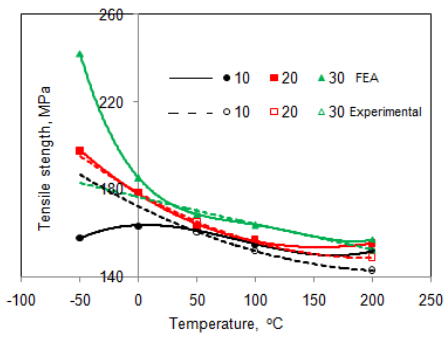

Fig. 6. Effect of temperature and volume fraction of Ni-coated B_4C nanoparticles on tensile strength.

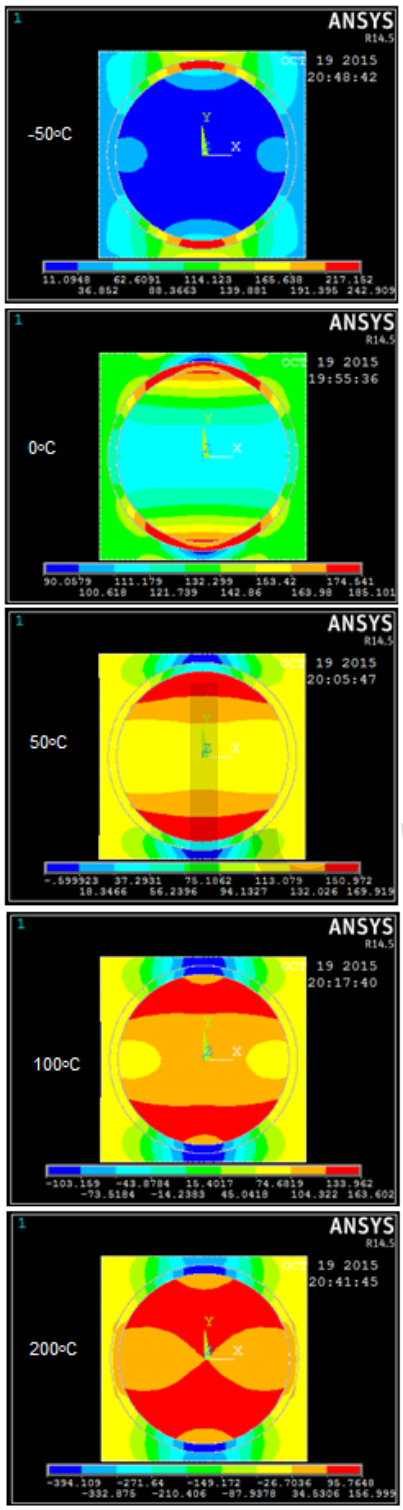

Fig. 7. Tensile strength induced in composites with30%Vp nanoparticles.

The tensile strength decreased with increase of temperature while it increased with increase of volume fraction of Ni-coated B_4C nanoparticles (figure 6). As the temperature increased the transfer of hydrostatic pressure was also transferred from the matrix to the nanoparticle (figure 7). The contour plots of the stress along the loading direction (figure 7) have shown that the high volume fraction of nanoparticles in the composite shared more loads when the composite subjected to the same external loading. As the temperature increased, the maximum stress occurred in the nanoparticle, which was consistent with other local stress observations.

The effect of temperature and volume fraction of Ni-coated B_4C nanoparticles on elastic modulus is shown in figure 8. It was observed that the effective elastic modulus of the composite increased with higher particle volume fraction and decreased with increase of temperature. The higher sensitivity occurred for particle volume fraction greater than 10%.

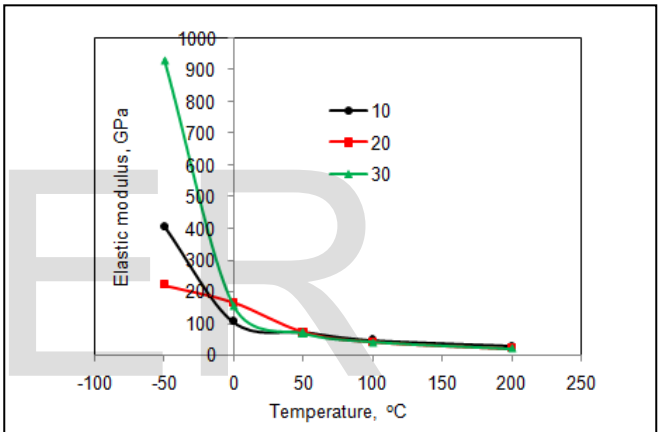

Fig. 8. Effect of temperature and volume fraction of Ni-coated B_4C nanoparticles on elastic modulus.

4.2 Fracture Behavior

The stress intensity increased at the interphase between the nanoparticle and the matrix as the temperature increased from -50°C to 200°C (figure 9). Within the nanoparticle various stress intensity contours were also observed due to CTE mismatch between B_4C nanoparticle Ni-coating and Aa1100 matrix. It was also noted that the maximum strain field in the vicinity of interphase was up to three to four times higher than that far away from the nanoparticle–matrix interfaces (figure 5). This high-strain region due to the interphase effect enlarged with the increase of nanoparticle content and temperature. This implies a potential early debonding [7]. The SEM images (figure 10) revealed the same trend in the composites. The sharp interphase boundary Ni_3Al was smeared out between the B_4C nanoparticle and the AA1100 matrix. At the subzero temperature, precipitates in the diffusion zone were clearly visible in the optical microscope. As the temperature increased ductile mode of failure was witnessed in the composites. Some

structural changes were locally occurred on the surface of the B_4C nanoparticle. At subzero temperature the failure mode was brittle in nature.

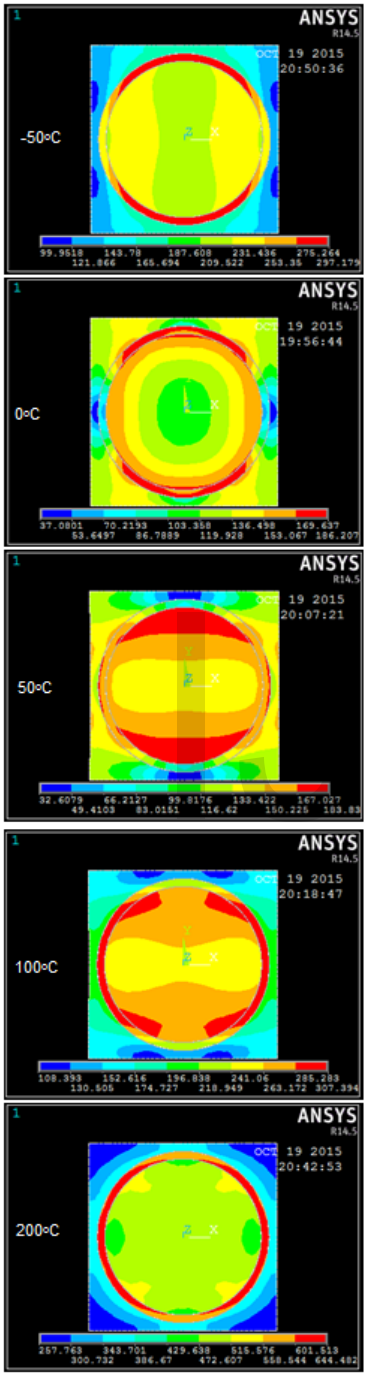

Fig. 9. Stress intensity induced in composites with30%Vp nanoparticles.

5. Conclusions

The thermo-elastic strain increased with increase of temperature of three-phase AA1100/Ni-coated B_4C metal matrix composites. As the temperature increased, the maximum stress occurred in the nanoparticle. the effective elastic modulus of the composite increased with higher particle volume fraction and decreased with increase of temperature. The failure modes were ductile type and brittle type, respectively, at high and subzero temperatures..

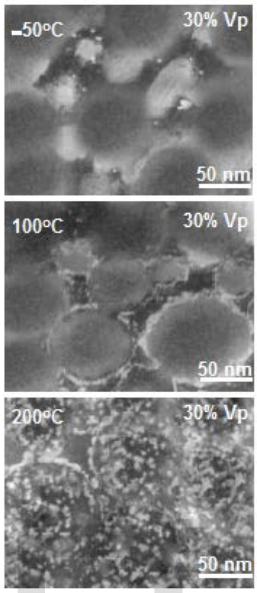

Fig. 10. Fracture mode in AA1100/Ni-coated B_4Ccomposites.

Acknowledgement

The author is thankful to University Grants Commission (UGC), New Delhi for sponsoring this project.

References

[1] A. Chennakesava Reddy, "Mechanical properties and fracture behavior of 6061/SiCp Metal Matrix Composites Fabricated by Low Pressure Die Casting Process," Journal of Manufacturing Technology and Research, vol.1, pp. 273-286, 2009.

[2] A. Chennakesava Reddy and Essa Zitoun, "Tensile properties and fracture behavior of 6061/Al_2O_3 metal matrix composites fabricated by low pressure die casting process," International Journal of Materials Science, vol.6, pp. 147-157, 2011.

[3] I. Doghri and C.Friebel, "Effective elasto-plastic properties of inclusion reinforced composites. Study of shape, orientation and cyclic response," Mechanics of Materials, vol.37, pp.45–68, 2005,

[4] D. Duschlbauer, H.J. Bohm and H.E. Pettermann, "Computational simulation of composites reinforced by planar random fibers: Homogenization and localization by unit cell and mean field approaches," Journal of Composite Materials, vol.40, pp.2217–2234, 2006.

[5] A. Chennakesava Reddy, "Influence of Interphase on Tensile Behavior of Strain Hardened AA1100/AlN Nanocomposites Using RVE Models and Experimental Validation," International Journal of Engineering, Science and Technology, vol.7, pp.239-250, 2015.

[6] A. Chennakesava Reddy and Essa Zitoun, "Matrix Al-alloys for alumina particle reinforced metal matrix composites," Indian Foundry Journal, vol.55,pp. 12-16, 2009

[7] M.J. Mahmoodi, M.M.Aghdam and M. Shakeri, "Micromechanical modeling of interface damage of metal matrix composites subjected to off-axis loading," Material Design, vol.31, pp.829–36, 2010.